Energy Estimation of Brushed DC Motor in Electric Vehicle by Finite Element

K. Lonphan[1] and S. Ruangsinchaiwanich[1,*]

ARTICLE INFO

Article history:
Received: 19 June 2025
Revised: 28 November 2025
Accepted: 11 February 2026
Online: 20 July 2026

Keywords:
Energy estimation
Brushed DC motor
Finite element

ABSTRACT

Recently, electric vehicles have attained global prominence as a viable alternative to traditional oil-powered automobiles. It is essential to recognize that electric vehicles employ distinct automotive technologies, in contrast to traditional vehicles. The motors that power an electric vehicle substantially affect its performance. This work presents a finite element method framework designed to investigate and evaluate the energy efficiency of a brushed DC motor within an electric bicycle application. We focus on evaluating its energy usage through a case study conducted at Pibulsongkram Rajabhat University (PSRU) in Phitsanulok Province, Thailand. A comparison can thus be made between the energy consumption estimated by the experimental work (EW) and the finite element evaluation (FE). Consequently, the error is 10.92 percent in their comparison.

1. INTRODUCTION

Transportation, which includes cars, trucks, and buses, is the major cause of contamination in some areas, for example, the Mid-Atlantic region in particular. Although electric vehicles are among the most promising technologies for reducing petroleum fuel consumption, moderate- and low-income users who normally travel short distances share in these consumer benefits. In Thailand, many universities are encouraged to be green universities; therefore, either bicycles or electric bicycles are motivated to be consumed and used to avoid increasing pollution. Furthermore, governments globally are advocating for cycling as a sustainable mode of transportation, and bike-sharing programs have become widely embraced in urban public transit owing to their convenience and ecological advantages recently [1]. Furthermore, it can expand mobility around busy city routes. The identification of locations for new stations is vital for network growth; nevertheless, some pattern examinations, for example, the spatial-temporal memory network, are necessary for precise identification of these places [2]. In addition, implementing Narrowband Internet of Things (NB-IoT) technology for device-to-server communication within user-identifying smart locks can lead to substantial financial expenditures [3].

In Europe, sales of electric bicycles rose steadily last year. There has been consistent growth in the market for electric bicycles since their introduction in the early 2000s, and experts predict that sales in Europe will continue at a rate of 30% per year [4]. Between 2019 and 2024, the global electric bicycle market was projected to expand at a compound annual growth rate (CAGR) of 6.39%, rising from a baseline valuation of $14,755.20 million [5]. Because of its widespread acceptance as a convenient last-mile alternative to conventional public transportation, it is ideal for shorter distances and point-to-point trips. Moreover, by 2019, Shanghai's dockless bike-sharing system had 305 thousand registered bicycles and was generating one million rides daily on average [6]. The rapid expansion of bike-sharing systems within Lanzhou's central business district has introduced spatial oversaturation [7], unregulated market rivalry, poorly defined parking zones, and severe traffic gridlock. To optimize this infrastructure, a dedicated feedback platform capable of instantaneous data acquisition, categorization, evaluation, and remediation is indispensable.

Numerous literary works have recently been published, concentrating on the modeling of electric bicycles (e-bikes). A research study develops an analytical model of the e-bike that precisely mirrors the motorcycle, incorporating its kinematics and dynamics [8]. Therefore, the model is subsequently estimated for speed tracking and distance traveled to ascertain its effectiveness. The results illustrate the distinct capabilities of the created model to monitor the speed profile. The distance covered by the e-bike model may be precisely evaluated. Currently, a significant difficulty in transport electrification also involves decreasing the size and weight of components to enhance power density [9]. The goal is frequently accomplished by engineering electrical devices with elevated rotational speeds and excitation frequencies. Either an analytical method or the finite element (FE) can evaluate electric losses, for example, winding copper loss, eddy current loss in the motor [10, 11].

[1]*Department of Electrical and Computer Engineering, Faculty of Engineering, Naresuan University, Phitsanulok, 65000, Thailand.*
**Corresponding author:* S. Ruangsinchaiwanich; Phone: +66-869-255-005; Email: sompornr@nu.ac.th.

This paper evaluates the energy consumption of an electric vehicle's brushed DC motor by analyzing its electrical characteristics, specifically efficiency and output power, via finite element analysis (FEA). Owing to its precision, versatility, and practical utility in modeling complex physical geometries, FEA serves as an indispensable tool for engineers and physicists alike. Furthermore, we concentrate on assessing its energy consumption based on a case study performed at Pibulsongkram Rajabhat University (PSRU) in Phitsanulok Province, Thailand, as illustrated in Figure 1, where the Talay Kaew region covers roughly 160,000 square meters, designating it an appropriate site for electric vehicles.

Fig. 1: Top map of Pibulsongkram Rajabhat University.

2. BRUSHED DC MOTOR

The performance of an electric vehicle is contingent upon its motor. A variety of motors are chosen to determine the engine capacity of the electric car. Trivial electric vehicles often employ with a brushed DC motor. Furthermore, the motor is predominantly used for generating continuous motion, and their rotational speed may be effectively regulated, rendering them suitable for applications necessitating speed control. A brushed DC motor generally comprises two primary components: a stator, which serves as the stationary element utilizing permanent magnets, and a rotor, which functions as the spinning component equipped with armature coil windings. Additionally, brushes serve as electrical contacts affixed to the outside frame, making contact with the commutator's contact points on the rotor's moving shaft to transmit power to the coil wires. The electric current in these wires generates a magnetic field that exerts a force on the stationary permanent magnets of the motor's immobile structure.

The force exerts pressure on the winding wire, resulting in the rotation of the rotor. As the rotor/armature rotates, the commutator contacts transition from one brush to the other, altering the current's polarity in the winding and consequently the magnetic field's polarity. A wire that first approaches a magnet and repels it subsequently becomes attracted to that magnet; after it surpasses the magnet, the current's direction reverses, resulting in the wire being repulsed by the proximal magnet and attracted to the distal one. This cycle replicates four times each spin due to the presence of four external magnetic poles.

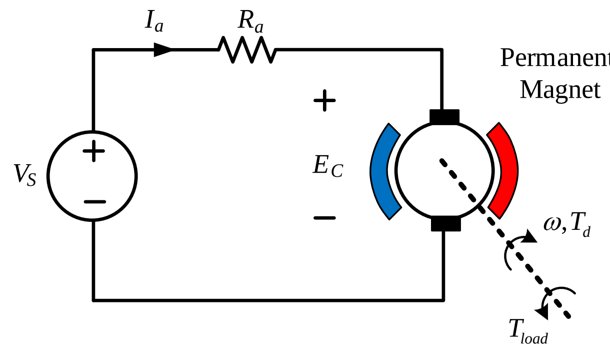

Fig. 2: Schematic diagram of the PM brushed DC motor equivalent circuit.

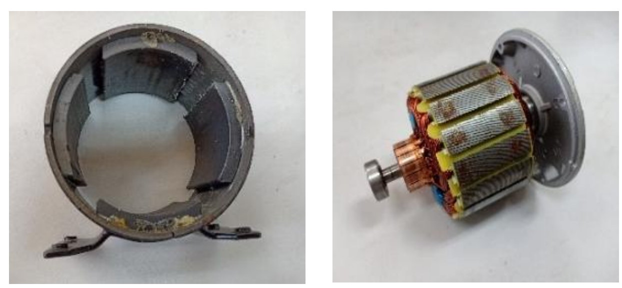

(a) Permanent magnet poles

(b) Armature winding

Fig. 3: PM brushed DC motor components.

Initially, the steady-state equivalent circuit of the brushed DC motor is introduced in Figure 2. To complement this, Figure 3 illustrates the internal constituents of the machine, such as the armature winding and permanent magnet poles. Consequently, the core efficiency of this motor can be evaluated according to [14].

Back EMF (E_c):

$$E_c = k_c \omega \tag{1}$$

where, k_c is constant of back EMF (V/rad/s); ω is angular frequency (rad/s)

Armature current (I_a):

$$I_a = \frac{V_S - E_c}{R_a} \tag{2}$$

where, V_S is DC power supply, R_a is armature resistance.

Gross power developed (P_e) by armature:

$$P_e = E_c I_a = k_c \omega I_a \tag{3}$$

Net mechanical output power (P_{out}),

$$P_{\text{out}} = P_d = \omega T \tag{4}$$

Input power (P_{in}),

$$P_{\text{in}} = V_S \times I_a \tag{5}$$

$$P_{\text{in}} = P_{out} + \text{Losses}_{\text{total}} \tag{6}$$

Efficiency (η) of motor,

$$\eta = \frac{P_{\text{out}}}{P_{\text{in}}} \tag{7}$$

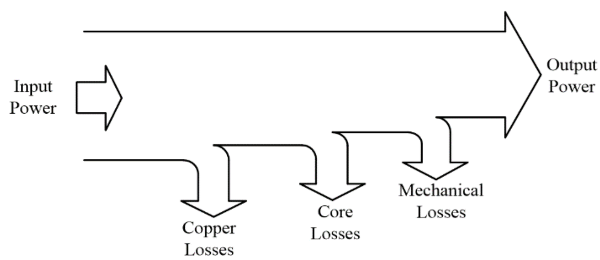

Fig. 4: Power flow diagram of a DC motor

Fundamentally, the estimation of core loss relies on the intensity of the magnetic field and the rotor velocity. The square of the armature current, along with the armature resistance, dictates the armature copper loss in a PM brushed DC motor. Moreover, windage loss, friction loss, rotational loss, and stray load loss, which are challenging to quantify and represent minor value losses, might be aggregated as mechanical losses. Figure 4 illustrates a conventional power flow diagram of a DC motor [14]. Equation (5) computes a segment of the input power derived from the voltage input and the input current. The residual power is the energy supplied to the armature, a fraction of which is dissipated as core loss in the armature core and copper loss in the armature windings. Moreover, remaining power refers to the gross mechanical power generated, of which a fraction is dissipated as friction, while the remaining power is the net mechanical power augmented. Equation (7) establishes the operational efficiency of this DC motor by correlating its power output with the total input energy.

The global revival of cycling has accelerated the market penetration of electric bicycles, which function as conventional cycles enhanced by battery-driven propulsion systems. Despite its batteries, it ranks as one of the most geologically sustainable forms of transportation, next walking and conventional cycling. Figure 5 illustrates the e-bike prototype, which was engineered using a conventional bicycle to mitigate mechanical losses. The prototype features a 350-watt permanent magnet brushed DC motor, as illustrated in Figure 3. The circuit connection for the experiment begins with two 12V 21A lead-acid batteries connected in series to provide a 24V 21A power supply. An energy meter is then connected to the battery to measure power and energy consumption. The output of the energy meter is connected to a motor speed controller to regulate the voltage appropriately for sending to the brushed DC motor according to the desired electric bicycle speed.

Fig. 5: Electric Bicycle.

Table 1: DC Motor Parameters

Parts	Prameter	Value
Stator	Outer Diameter	100 mm
	Inner Diameter	82 mm
	Length	60 mm
	Steel Type of the Stator Core	Steel_1008
	Magnet Type	Alnico9
	Magnet Length	50 mm
	Magnet Thickness	5 mm
Rotor	Outer Diameter	80 mm
	Inner Diameter	10 mm
	Length	38 mm
	Steel Type of the Rotor Core	Steel_1008
	Number of Slot	16 Slot

3. THE FINITE ELEMENT METHOD

The finite element method (FEM) is a multifaceted numerical technique employed to model diverse physical processes. Many engineers utilize it to reduce the quantity of physical prototypes and tests while examining variables in their design domain to enhance product quality. The transient two-dimensional FE analysis is employed to evaluate and analyze motor performance. To model motion within the motor's transient finite element framework, an electromagnetic formulation incorporating velocity is essential. According to established electromagnetic principles [15, 16], accounting for the velocity term in a stationary reference frame results in the following governing relation:

$$\nabla \times \left(\frac{1}{\mu} \nabla \times \vec{A} \right) + \sigma \left(\frac{\partial \vec{A}}{\partial t} - \vec{v} \times (\nabla \times \vec{A}) \right) = \vec{J}_0 \qquad (8)$$

In this formulation, μ and $\vec{A}$ correspond to the magnetic permeability and magnetic vector potential, respectively, whereas σ, $\vec{J}_0$, and $\vec{v}$ denote the material's electrical conductivity, applied source current density, and velocity.

The velocity term can be effectively eliminated by dynamically shifting the rotor mesh, which consequently reduces the velocity to zero relative to the moving frame of reference. Represented in both the stator's stationary framework and the rotor's moving reference frame, Equation (8) yields the following general formulation, consistent with:

$$\nabla \times \left(\frac{1}{\mu} \nabla \times \vec{A} \right) + \sigma \left(\frac{\partial \vec{A}}{\partial t} \right) \approx \vec{J}_0 \qquad (9)$$

Spatial discretization via the weighted residual method transforms the aforementioned field equations into matrix form. Concurrently, the field, circuit, and mechanical motion formulations undergo discretization within the time domain.

The determination of the approximate solution using the finite element method, domain, or region surface of the geometry of the motor on the x-y plane is examined. The mathematical model of the electromagnetic field for a linear 2-D Cartesian can be shown in the second-order differential equation as:

$$\frac{\partial}{\partial x}\left(\frac{1}{\mu} \frac{\partial A}{\partial x} \right) + \frac{\partial}{\partial y}\left(\frac{1}{\mu} \frac{\partial A}{\partial y} \right) - i\omega\sigma A = -J_0 \qquad (10)$$

where, A and μ correspond to the unknown magnetic vector potential and magnetic permeability, respectively; whereas σ, ω, J_0, and i denote the material's electrical conductivity, angular velocity, applied external current density, and the imaginary component.

4. FEM SIMULATION RESULTS AND ENERGY ESTIMATION

A FEM simulation of the DC prototype motor was indicated by using the parameters specified in Table 1 from the previous section. Principally, the stator outer diameter is 100 mm, the rotor diameter is 80 mm, the air gap has a minimum radial dimension of 2 mm. The rotor has 16 slots for inserting armature winding and the stator has 4 permanent magnet poles. Furthermore, a 2D representation of the magnetic fields of the FEM-simulated motor with steady-state levels was illustrated in Figure 7.

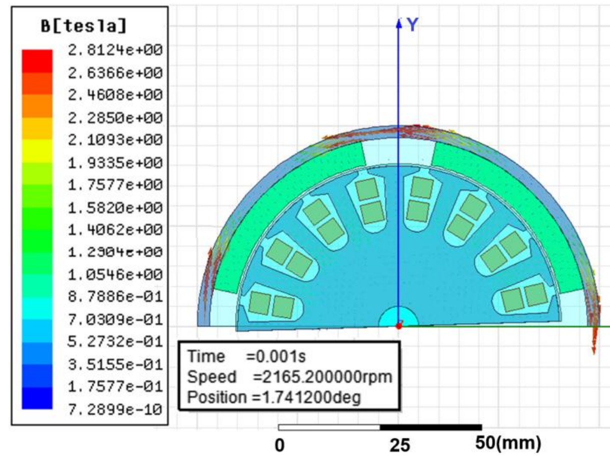

Fig. 7: 2D cross-sectional representation of the DC motor via finite element analysis.

As demonstrated in Figure 8, the computational output power is verified for rotational velocities ranging between 0 and 4,000 rpm. Correspondingly the maximum predicted output power was 350 W. Certainly, it is typically represented by a classic parabolic curve. Additionally, the motor's power is contingent upon both speed and torque; power is diminished when speed is elevated and torque is minimal [13]. The converse is also valid: when speed is diminished and torque is elevated, power will likewise be reduced. This indicates that power often reaches its zenith at the halfway between maximum velocity and the stall threshold. In addition, because the FEM simulation and the magnetic circuit parameters do not match perfectly, determining the exact source of this inconsistency poses a significant challenge.

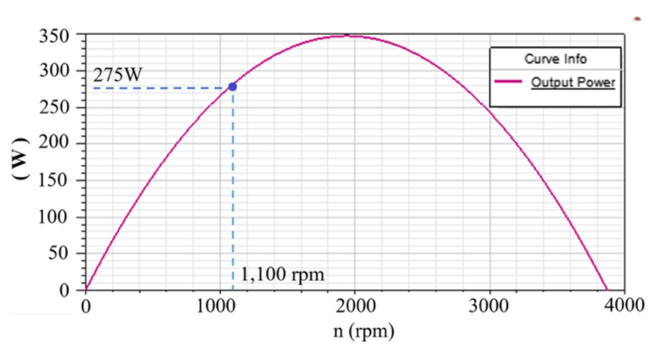

Fig. 8: Output power profiles evaluated across different rotor rotational velocities.

The anticipated travel distance to the university is approximately 5 kilometers, as depicted in Figure 9, which outlines the route plan for the experiments undertaken in this study. The electric car prototype achieves an average velocity of 19 km/hour, equating to a motor speed of approximately 1,100 rpm. The finite element study revealed that the motor prototype incurred losses, including a core loss of 6.38 watts and a maximum armature copper loss of 97.01 watts. The output power is predicted to be roughly 275 watts, as illustrated in Figure 8.

Physically, frictional and windage losses arise from the friction between the shaft and bearings, referred to as rotational losses. The windage loss fundamentally relies on the design and configuration of the rotating object. Verifying the windage loss of the electric rotating machine using the finite element method is complex. In the analytical method, friction and windage losses can be estimated at roughly 1% of the complete load loss or disregarded entirely [12] that for this energy estimation is proposed to neglect.

Subsequently, the total losses can be estimated using in the equation (6), and it can be computed as:

$$\begin{aligned} \text{Total losses} &= \text{core loss} + \text{armature copper loss} \\ &= 6.38+97.01(275/350) \\ &= 82.59 \text{ W} \end{aligned}$$

Consequently, the input power can be estimated using in the equation (7), and it can be computed as:

$$P_{in} = P_{out} + \text{Total loss} ==275+82.59 =357.59 \text{ W}$$

Consequently, this propose utilizes the finite element method in order to obtain an estimate of the amount of energy that the electric bicycle is able to consume. In Figure 8, they have been taken into consideration. Additionally, we are able to process the energy usage per distance using units of kilowatt-hours (kWh). Because of this, the energy consumption of the finite element (EC-FE) can be approximated using the following formula:

$$\text{FC-FE} = 19.50 \text{ km} / 357.59 \text{ Wh} = 54.53 \text{ km/Wh}$$

5. EXPERIMENTAL ENERGY ESTIMATION

At this point in the project, the electric bicycle prototype was achieved available for proceeding in the Pibulsongkram Rajabhat University campus in TaLe Kaew area. As can be seen in Figure 9, the yellow line was objective used to illustrate the layout of this study, and it indicates that the projected travel distance is around 5 kilometers based on the local road that surrounds the institution. In addition, it is essential to mandate that there be a comparable electricity load for students who are volunteering their time and who weigh close to 65 kg. The power meter, which is used to monitor the electric parameters, and other meters, such as a digital timer and a distance meter, are therefore identified with these useful collections in order to facilitate subsequent statistical analysis.

Figure 10 illustrates the resultant speed that the red line signifies speed with km/hour units upon the application of a direct current voltage of approximately 25 volts. We recorded a motor speed of around 1,121 revolutions per minute (rpm.). The acquired power data is presented in Figure 11. The direct current power ranges as shown in the blue line controlled at levels from 0 watts to 620 watts.

Fig. 9: Distribution map of this study case.

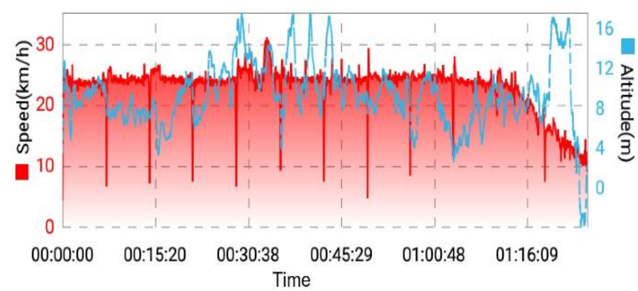

Fig. 10: Speed recording.

In this circumstance, given the prolonged operation of the motor and its association with multiple functions, it should be managed appropriately to ensure variability and maintain overall motor health. It is crucial to acknowledge that decreasing the proximity to the ideal efficiency point will result in an increased current draw and an elevated danger of premature failure. It is highly recommended that the motor not be operated continuously at elevated power levels. Should this transpire, the motor would swiftly overheat, hence increasing the likelihood of damage to the motor windings.

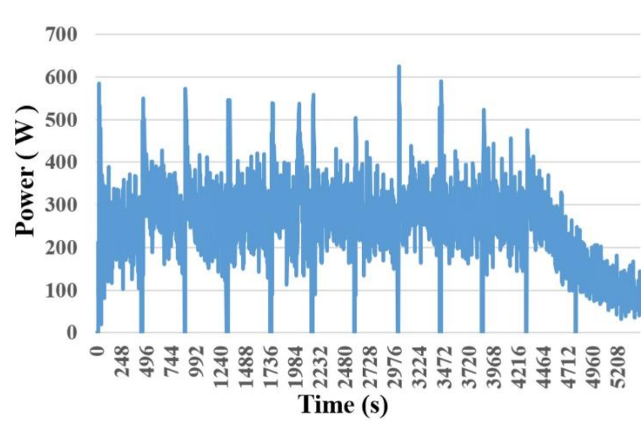

Fig. 11: Power recording.

Table 2: Experimental driving test

Parameters	Test			average
	1	2	3	
Length (km)	5.012	5.016	5.015	5.013
Duration (s)	912	932	942	927.6
Average speed (km/h)	19.78	19.38	19.17	19.50
Maximum speed (km/h)	24.63	23.23	25.62	24.72
Average speed motor (rpm)	1,137.82	1,114.81	1,102.73	1,121.94
Average voltage (V)	25.84	25.92	25.96	25.88
Average ampere (A)	15.32	15.24	15.42	15.30
Average power input (W)	395.87	395.02	400.30	395.85
Energy consumption (Wh)	100.28	102.27	104.75	101.79

Data acquired from the experimental driving test are equivalent, as illustrated in Table 2, due to the fact that the electrical load and distance are both limited. A cyclist with a mass of 65 kg was utilized in the experiment. Three experiments were performed under actual traffic conditions to determine the average value and document numerous parameters, including distance, trip time, average speed, maximum speed, voltage, current, input power, and energy consumption. The energy consumption of the experimental work (EC-FW) can be estimated using the subsequent formula:

$$EC\text{-}EW = 5.013 \text{ km} / 101.79 \text{ Wh} = 49.24 \text{ km/Wh}$$

Table 3: Comparison of energy consumption

Parameters	EW	FE
Energy Consumption (km/ kWh)	49.24	54.53
Energy Cost (Baht/km)	0.063	0.072

Table 3 confirmations comparison of the resultant energy consumption to estimate by the experimental work (EW) and the finite element (FE). Consequently, the percentage error can be calculated as 10.92 percent. Energy cost of this electric bicycle prototype are established correspondingly. In order to reduce living costs, electric bicycle is potential comparing with other vehicles.

6. CONCLUSION

This study aims to evaluate the performance of an electric bicycle's brushed DC motor by implementing a finite element methodology. An analysis of the case study that was developed for the purpose of conducting research at Pibulsongkram Rajabhat University is the primary focus of the assessment of its energy consumption. It is therefore possible to make a comparison between the consequent energy consumption that was estimated by the experimental work (EW) and the finite element evaluation (FE). Therefore, the error is 10.92 percent for their comparison. Essentially, the finite element approach is able to conform to varied simulation, and it is accomplished by comparing the findings of the analysis with the work that was done in the experiment. However, students who wish to learn how to apply the finite element technique to their own interests need to be careful during the setting process. Otherwise, results of the finite element method can be questioned. Future research should investigate another category of electric motor frequently utilized in electric bicycles: the brushless DC motor. This motor possesses multiple advantages, such as the absence of brush losses, elevated efficiency and torque, and an extended service life. This type can decrease energy usage in electric bicycles, allowing for extended travel range.

ACKNOWLEDGMENT

Acknowledgment is gratefully extended to both the Faculty of Engineering at Naresuan University and Pibulsongkram Rajabhat University for their institutional support in providing research devices. Furthermore, this research was funded by Naresuan University via the National Science, Research, and Innovation Fund (Grant Number: R2563B007).

REFERENCES

[1] Lu, H.; Zhang, M.; Su, S.; Gao, X.; and Luo, C. 2019. Broken Bike Recycling Planning for Sharing Bikes System. IEEE Access 7 :177354-177361.

[2] Li, X.; Xu, Y.; Chen, Q.; Wang, L.; Zhang, X.; and Shi, W. 2022. Short-Term Forecast of Bicycle Usage in Bike Sharing Systems: A Spatial-Temporal Memory Network. IEEE Transactions on Intelligent Transportation Systems 23(8): 10923–10934.

[3] Xue, Z.; Lin, L.; Ma, Y.; Dou, Z.; Zhao, Y.; Zhang, Y.; and Zhang, X. 2020. A Shared Bicycle Intelligent Lock Control and Management System Based on Multisensor. IEEE Internet of Things Journal 7(6): 5426–5433.

[4] Xue, Z.; Lin, L.; Ma, Y.; Dou, Z.; Zhao, Y.; Zhang, Y.; and Zhang, X. 2020. A Shared Bicycle Intelligent Lock Control and Management System Based on Multisensor. IEEE Internet of Things Journal 7(6): 5426–5433.

[5] Efken, M.; Kohn, N.; Greven, D.; and Misgeld, B.J.E. 2021. Cooperative control of electrical bicycles. IFAC Journal of Systems and Control 16: 100153.

[6] Mordor Intelligence. E-bike Market - Growth, trends, and forecast. Accessed on 14 January 2023 from https://www.mordorintelligence.com/industry-reports/e-bikemarket.

[7] Yu, Q.; Xie, Y.; Li, W.; Zhang, H.; Liu, X.; Shang, W.; Chen, J.; Yang, D.; and Yan, J. 2022. GPS data in urban bicycle-sharing: Dynamic electric fence planning with assessment of resource-saving and potential energy consumption increasement. Applied Energy 322: 119533.

[8] Ji, W.; Lu, C.; Mao, J.: Liu, Y.; Hou, M.; and Pan, X. 2021. Public's Intention and Influencing Factors of Dockless Bike-Sharing in Central Urban Areas: A Case Study of Lanzhou City, China. Sustainability 13(6): 9265.

doi.org/10.3390/su13169265.

[9] Hanifah, R.A.; Toha, S.F.; Hanif, N.H.H.M.; and Kamisan, N.A. 2019. Electric motorcycle modeling for speed tracking and range travelled estimation. IEEE Access 7: 26821-26829.

[10] Srivichai, J.; Ratniyomchai, T.; and Kulworawanichpong, T. 2021. Modelling and Analysis of Voltage Distribution for Automated People Mover System in a Case Study of Suranaree University Technology Hospital Shuttle Service. GMSARN International Journal 15(1): 12-20.

[11] Preci, E.; Valente, G.; Galassini, A.; Yuan, X.; Degano, M.; Gerada, D.; and Gerada, C. 2020. Experimental statistical method predicting AC losses on random windings and PWM effect evaluation. IEEE Transactions on Energy Conversion 36(3): 2287-2296.

[12] Kim, D.M.; Kim, J.H.; Lee, S.G.; Park, M.R.; Lee, G.H.; and Lim, M.S. 2020. Estimation method for rotor eddy current loss in ultrahigh-speed surface-mounted permanent magnet synchronous motor. IEEE Transactions on Magnetics 57(2): 1-5.

[13] Patel1, Amit N. 2024. Cogging Torque Minimization of Dual Rotor Axial Flux Permanent Magnet Brushless DC Motor Using Magnet Shifting Technique. GMSARN International Journal 18(3): 291-297.

[14] Chapman, S.J. 1999. Electrical Machinery Fundamentals. New York: McGraw Hill Companies Inc.

[15] Lipo, T.A. 1995. Finite Element Analysis of Electrical Machines. Boston: Kluwer Academic Publishers.

[16] Reece, A.B.J.; and Preston, T.W. 2000. Finite Element Methods in Electrical Power Engineering. Oxford: Oxford University press.